Cadmium-doping slows trap emptying in ambient-air blade-coated formamidinium lead iodide perovskite solar cells

Dongyang Zhang, Sutripto Khasnabis, Wanlong Wang, Vishal Yeddu, Shahram Moradi, Muhammad Awais, Hai-Dang Nguyen, Sean B. Reinecke, Yuki Haruta, Robert Godin, Furui Tan, & Makhsud I. Saidaminov

2024

ADVANCED ENERGY MATERIALS
www.advenergymat.de

Cadmium-Doping Slows Trap Emptying in Ambient-Air Blade-Coated Formamidinium Lead Iodide Perovskite Solar Cells

Dongyang Zhang, Sutripto Khasnabis, Wanlong Wang, Vishal Yeddu, Shahram Moradi, Muhammad Awais, Hai-Dang Nguyen, Sean B. Reinecke, Yuki Haruta, Robert Godin, Furui Tan,* and Makhsud I. Saidaminov**

Formamidinium lead iodide ($FAPbI_3$) in its α-phase is among the most desirable perovskite compositions for solar cells. However, because of its transition into the yellow δ-phase at room temperature, it is a challenge to process it in ambient air by scalable fabrication methods. Here the introduction of a trace amount of cadmium (in the form of CdI_2) to $FAPbI_3$ is reported and found that it enhances the stability of the perovskite's black α-phase polymorph, inhibits non-radiative recombination events, leads to pin-hole free compact surface morphology, and improves band energy alignment. The 0.6% Cd-doped $FAPbI_3$ solar cells show a champion efficiency of 22.7% for 0.049 cm^2 and 16.4% for cm^2-scale pixels, which, to the best of the knowledge, are among the highest for air-ambient fully blade-coated pure $FAPbI_3$ solar cells with an *n-i-p* architecture. Transient absorption microscopy measurements reveal that Cd doping reduces the number of trapped charges and increases their lifetimes, promoting charge accumulation and a higher photovoltage. The study sheds light on the potential of cadmium as a homovalent dopant for the stabilization and performance enhancement of $FAPbI_3$ performance solar cells.

1. Introduction

Formamidinium lead iodide ($FAPbI_3$) in its α-phase is arguably one of the most desired perovskite compositions for solar cells,[1–3] reaching a power conversion efficiency (PCE) of 26.1%. It offers a bandgap of ≈1.5 eV,[4,5] which is the lowest among known single-Pb-based perovskites and is closest to the ideal bandgap of 1.34 eV for single-junction solar cells (Shockley-Queisser limit).[6] Additionally, it exhibits improved thermal and operational stability compared to the archetypical $MAPbI_3$ perovskite (MA stands for methylammonium): $MAPbI_3$ decomposes at ≈100 °C,[7,8] whereas $FAPbI_3$ remains intact up to 170 °C.[9,10]

However, α-$FAPbI_3$ is metastable at room temperature and readily transforms into the undesired wide bandgap δ-phase; this phenomenon is known as

D. Zhang, V. Yeddu, H.-D. Nguyen, S. B. Reinecke, Y. Haruta, M. I. Saidaminov
Department of Chemistry
University of Victoria
Victoria, British Columbia V8P 5C2, Canada
E-mail: msaidaminov@uvic.ca

S. Khasnabis, R. Godin
Department of Chemistry
The University of British Columbia
Kelowna, British Columbia V1V 1V7, Canada
E-mail: robert.godin@ubc.ca

W. Wang, F. Tan
Laboratory of Photovoltaic Materials
Henan University
Kaifeng, Henan 475004, P. R. China
E-mail: frtan@henu.edu.cn

S. Moradi, M. Awais, M. I. Saidaminov
Department of Electrical and Computer Engineering
University of Victoria
Victoria, British Columbia V8P 5C2, Canada

R. Godin
Clean Energy Research Center
University of British Columbia
2360 East Mall, Vancouver, British Columbia V6T 1Z3, Canada

M. I. Saidaminov
Centre for Advanced Materials and Related Technologies (CAMTEC)
University of Victoria
Victoria, British Columbia V8P 5C2, Canada

The ORCID identification number(s) for the author(s) of this article can be found under https://doi.org/10.1002/aenm.202303858

DOI: 10.1002/aenm.202303858

polymorphism. The kinetics of $FAPbI_3$ polymorphism transformation is significantly affected by ambient conditions; for example, the humidity of ambient air accelerates this process.[1,11–13] Stabilization of α-$FAPbI_3$ with minor additives and interfacial layers with almost no increase in its bandgap has enabled record-breaking efficiencies in lab-scale perovskite solar cells (PSCs) fabricated by spin-coating in an inert environment.[14–29]

The spin-coating method is, unfortunately, neither economical (≈1% perovskite atom economy, see Supplementary Note 1, Supporting Information) nor scalable (each point on the substrate is affected by different magnitudes of centrifugal force, solution viscosity, and surface tension, leading to non-uniform films at multi-centimeter scales).[30,31] In contrast, commercially viable processes demand near-unity perovskite atom efficiency and uniform films at large scale. Blade-coating has recommended itself as one such alternative for scaling PSCs.[32]

Given the advantages of $FAPbI_3$ PSCs discussed above, it is now important to upscale them – a challenge yet to be addressed considering the $FAPbI_3$ polymorphism issue and its hypersensitivity to fabrication conditions.[33] Intermediate-phase engineering with the aid of N-Methyl-2-pyrrolidone has led to 17.8% efficient PSCs, a record value, to the best of our knowledge, among all blade-coated $FAPbI_3$ with *n-i-p* architecture.[33]

We recently reported that Pb-site doping effectively stabilizes α-$FAPbI_3$ single crystals.[34] Using Bi^{3+} as a dopant with smaller ionic radii than Pb^{2+}, we reported that this approach relaxed structural strain and stabilized the α-phase. But Bi^{3+}, unfortunately, introduced carrier recombination centers which we attributed to its heterovalent nature relative to Pb^{2+}. We thus hypothesized that introducing a homovalent Pb-site additive would overcome the issue.[35–37] One such alternative is cadmium (Cd^{2+}) – it is of the same oxidation state is a similarly soft Lewis acid as Pb^{2+}, and has a smaller atomic radius (0.95 Å vs 1.19 Å). The cadmium additive was shown to enhance the crystallinity of $MAPbI_3$, $CsPbIBr_2$, and $Cs_xFA_{1-x}PbI_3$ perovskite films and to suppress atomic vacancies via strain relaxation in triple-cation perovskites.[38–43] Cadmium's effect on the crystallinity of $FAPbI_3$, and its polymorphism, remains to be known.

Here we demonstrate that a trace amount of Cd indeed stabilizes α-$FAPbI_3$ enabling blade-coating of $FAPbI_3$ in ambient air. Using compositionally-graded film (CGF) optimization method,[44] we found that 0.6% Cd (relative to Pb) leads to the strongest photoluminescence of perovskite films. We then find that this exact composition also leads to the largest grain size in films with no pin holes. We also observe that Cd-doping enhances carrier lifetimes by an order of magnitude as compared to control $FAPbI_3$. Further photophysical investigations revealed that trap filling is promoted by Cd doping, leading to charge accumulation and higher photovoltage. Finally, we demonstrate all-blade coated $FAPbI_3$ solar cells reaching 22.7% power conversion efficiency.

2. Results and Discussion

We first fabricated $FAPbI_3$ film with the gradient content of Cd^{2+} via a CGF platform, as it allows making all possible binary compositions in a single experiment.[44] We showed earlier that the CGF composition changes linearly, i.e., one can accurately estimate a local composition from its location by $\frac{l}{L}(c_{ink1} - c_{ink2})$, where l is the distance from one end of the CGF film to the desired point, L is the length of the CGF (28 cm in this work), and c – the concentration additive in the inks.[44] For the CdI_2-$FAPbI_3$ CGF, the two $FAPbI_3$ inks with (5 mol. % CdI_2 relative to PbI_2) and without CdI_2 were deposited on a glass substrate by slot-die coater at varying ratios enabled by a gradual change of the pump rate of inks. The appearance of the resultant CGF film with gradient Cd composition is shown in **Figure 1a**.

To identify the optimal content of Cd, we measured the photoluminescence (PL) spectra (Figure 1b; Figure S1, Supporting Information) using a compact spectrometer with a reflection probe, which slid through the center of the film by a robotic arm and collected data at every 3 mm interval (corresponding to a spatial resolution of ≈0.05% Cd). The PL intensity increased along the film reaching the maximum intensity at l = 3.6 cm (corresponding to ≈0.6% concentration of Cd^{2+}) and then decreasing gradually. The enhancement of PL indicates the reduction of non-radiative recombination rate in the perovskite film, which is beneficial for the performance of solar cells.

To determine the impact of Cd on the morphology of perovskite films, we blade-coated $FAPbI_3$ films without and with CdI_2 on SnO_2-coated ITO (indium tin oxide)/glass substrates (we chose this substrate because it was used in solar cells discussed below). **Figure 2a** compares Scanning Electron Microscopy (SEM) images of the blade-coated films. The control $FAPbI_3$ film shows many pinholes, obscured grain boundaries as well as bright-contrast features on grains – all these defects may act as electron or hole recombination sites in the completed device. The size and density of grains increased with Cd doping and at 0.6% Cd reached full coverage, an important attribute for films in solar cells. Compact films and large grain sizes can effectively hinder the penetration of moisture and reduce the degradation caused by reactions between the grain boundaries and moisture.[45–49] Further addition of Cd over 1% led to a further increase in grain size but also resulted in poor coverage and large pinholes.

To understand how Cd-doping increases the grain size of $FAPbI_3$ film, we performed X-ray diffraction (XRD) characterization of as-deposited films before and after annealing, as well as dynamic light scattering (DLS) characterization of perovskite precursor inks. We observed stronger and more oriented diffraction peaks associated with FAI-PbI_2-solvent intermediate complexes in perovskite films containing Cd compared to those without Cd (Figure S2a, Supporting Information).[33] These complexes, when annealed, are known to produce highly crystalline perovskite films with enlarged grain size and fewer grain boundaries, as we also confirmed by SEM images (Figure 2a). Additionally, these complexes prevented the formation of δ-$FAPbI_3$, as observed in the XRD profiles of annealed films (Figure 2c, Figure S2b, Supporting Information).[50,51] DLS data of perovskite inks indicate that the average diameter of colloidal particles is ≈2 nm (Figure S3, Supporting Information). Furthermore, the colloids increase in size with a higher concentration of CdI_2. This reduces the number of nucleation sites, slowing down the nucleation rate during film formation.[43] XPS results in Figure S4 (Supporting Information) show the presence of Cd on perovskite films: the Cd $3d_{5/2}$ peak at ≈406 eV increases with higher Cd content in perovskite ink. Therefore, we

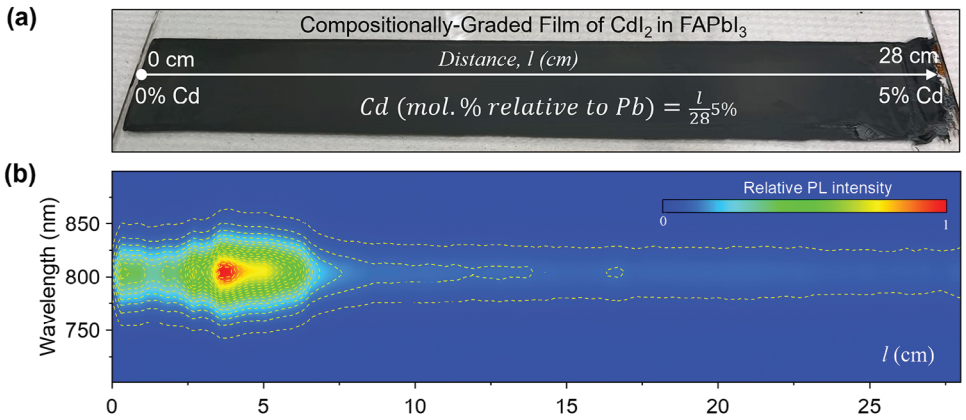

Figure 1. Compositionally-Graded Film (CGF) of CdI_2 and $FAPbI_3$: a) Image of the CGF film on a glass substrate with dimensions of 28 cm in length by 4 cm in width. b) Photoluminescence spectra in the color map along the CGF film at 3 mm intervals.

conclude that Cd strengthens the intermediate complexes, leading to larger grains, and completely prevents the formation of any δ-$FAPbI_3$.

A critical question, when doping a material, is determining the whereabouts of the dopant. One scenario involves dopant segregation, where Cd would manifest as CdI_2 or FA_2CdI_4 (a zero-dimensional structure with tetrahedral coordination of Cd) within the $FAPbI_3$ matrix.[52] To probe this scenario, we compared CdI_2 and FA_2CdI_4 XRD profiles with $FAPbI_3$ containing 0–20% CdI_2: at CdI_2 concentration of 5% and higher, we indeed observed diffraction peaks belonging to CdI_2 (Figure S6, Supporting Information); but at CdI_2 concentration of 1% and lower, we observed no discernible diffraction peaks corresponding to CdI_2 and FA_2CdI_4 (Figure 2c), ruling out the scenario of dopant phase segregation at the low dopant concentrations relevant to this study.

Another scenario entails dopant incorporation into the crystal structure, for which we have observed some evidence. First, we noted a change in full width at half maximum (FWHM) of XRD peaks when doping $FAPbI_3$ with cadmium. Lattice strain analysis using Williamson-Hall plots based on the XRD FWHM indicates that structural strain decreases to the minimum with the addition of 0.6% Cd (Figure S6, Supplementary Note 2, Supporting Information). Second, XPS results showed a shift of Pb $4f_{7/2}$, Pb $4f_{5/2}$ and I $3d_{5/2}$ in Cd-doped films indicating change in the environment of these elements (Figure S4, Supporting Information). Third, we grew $FAPbI_3$ single crystals with and without CdI_2. Using optimal Cd concentration in mother solutions, we observed the formation of only black $FAPbI_3$ phase, whereas without Cd, the yellow phase was dominant (Figure S7, Supporting Information). We then isolated the crystals, fully converted them to black phase through annealing, and left them in ambient air: after 46 days, the control $FAPbI_3$ crystals turned yellow, while $FAPbI_3$ with optimal Cd doping remained black (Figure S7, Supporting Information). The observed Cd effect on $FAPbI_3$ polymorphism should be due to its incorporation into crystal structure as single crystals are free of grain boundaries. In light of these observations, and Cd^{2+} and Pb^{2+} similar chemical properties (same oxidation state and Lewis acidity), we speculate that Cd^{2+} substitutes Pb^{2+} in $FAPbI_3$, at least at the concentrations tested here. It is worth noting that dopant incorporation into the crystal structure should lead to changes in lattice parameters and, consequently, shifts in XRD peaks. However, assuming substitutional doping of Pb (1.19 Å) with Cd (0.95 Å), a 0.6% Cd doping would result in a diffraction peak shift of only 0.003 °, a value that is practically challenging to resolve.

The UV-vis absorption spectra show a ≈1.5 eV bandgap with no appreciable change in the band edge with Cd doping (Figure 2b). The absorption slope and tail also remained unchanged, indicating that the Urbach energy, a measure of energetic disorder, remained the same. The enhancement in the intensity of absorption peak for the 0.6% Cd-doped $FAPbI_3$ is attributed to the compact, pin-hole-free nature of the film.

We also assessed the stability of the films. After aging in ambient air for 30 days at an RH of 35%, the $FAPbI_3$ film with no Cd predominantly exhibited the δ-phase, while the optimal Cd-doped samples showed no sign of degradation (Figure 2d; Figure S8, Supporting Information). Thus, we conclude that Cd doping effectively released the structural strain of the $FAPbI_3$ perovskite and stabilized its desired α-polymorph.[53–57]

Inspired by these findings, we used 0.6% Cd doped 1 M $FAPbI_3$ solutions to fabricate PSCs in Glass/ITO/SnO_2/$FAPbI_3$/Spiro-OMeTAD/Au configuration on 3.25 cm by 7.5 cm substrates in ambient air using air knife-assisted blade-coating method; SnO_2 and Spiro-OMeTAD layers were also deposited by blade coating method in ambient air at an RH of 35%; the gold counter-electrode was deposited by thermal evaporation. We report statistical data in Figure S9 (Supporting Information). The performance of champion PSCs for 0.049 cm^2 pixels, both with and without Cd, is shown in **Figure 3a**. The cell without Cd showed a PCE of 20.8% with a short-circuit current (J_{SC}) of 25.2 mA cm^{-2}, open-circuit voltage (V_{OC}) of 1.05 V, and a fill factor (FF) of 78.5%. Cd-doped one showed an increased PCE of 22.7% with a J_{SC} of 25.9 mA cm^{-2}, V_{OC} of 1.10 V, and FF of 79.6%. Control $FAPbI_3$ showed poor reproducibility due to the presence of pinholes, while >80% of target Cd-$FAPbI_3$ showed a PCE of over 20% (Figure 3b). Solar cells of 0.9 cm^2 active area with and

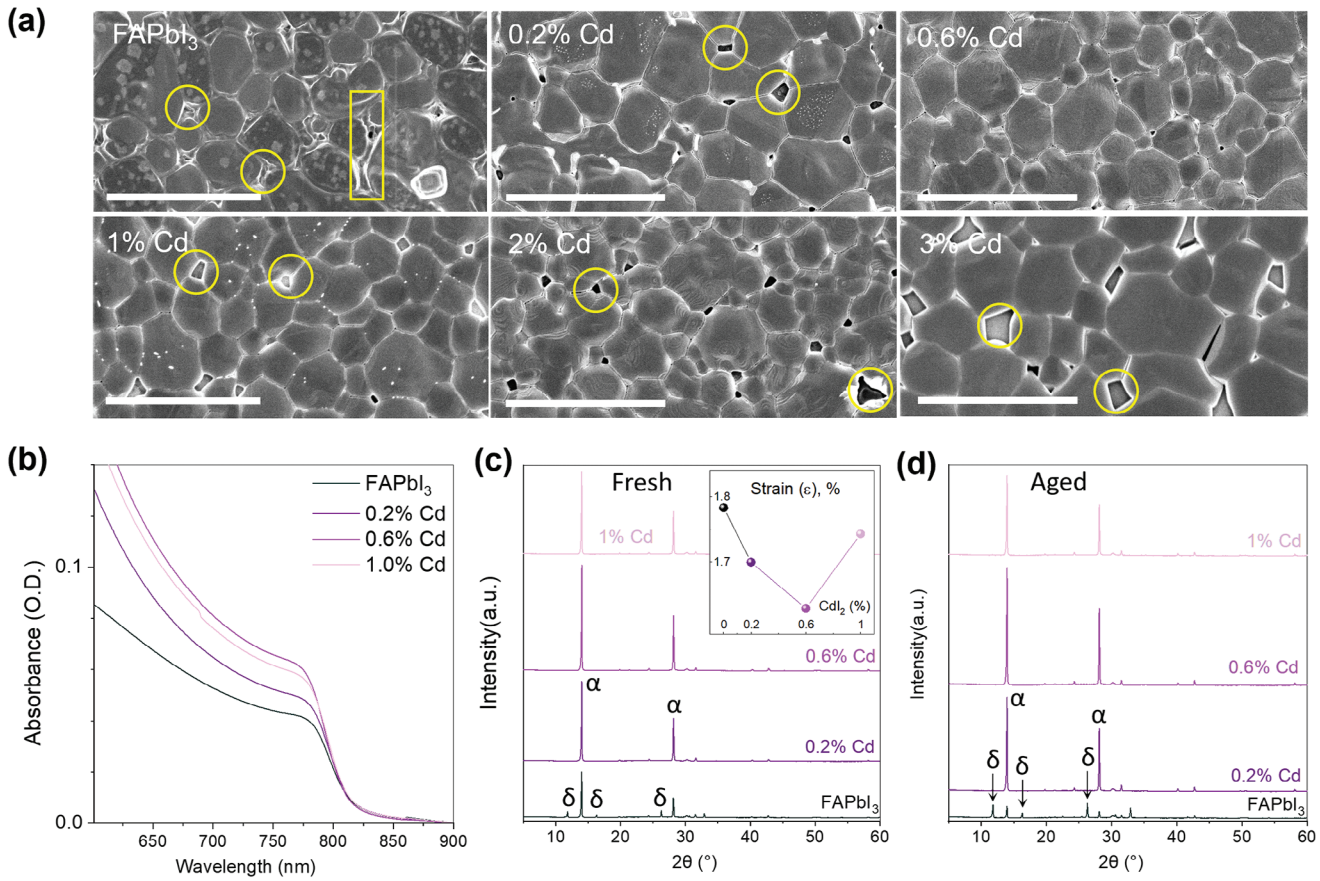

Figure 2. Characterization of Cd-$FAPbI_3$ blade-coated thin films. a) Surface SEM images. The scale bar indicates a length of 5 µm. The yellow rectangles and circles show pinholes and obscured grain boundaries. b) Absorption spectra of films. c) XRD profile of fresh films. d) XRD profile of films aged for 30 days in ambient air at relative humidity (RH) of 35%.

without Cd showed a champion PCE of 16.41% and 13.90%, respectively (Figure S10 and Table S1, Supporting Information). Major improvement in performance arises from V_{OC}. We also investigated the stability of unencapsulated PSCs. Consistent with the discussions above, Cd-$FAPbI_3$ solar cells retained 80% of their original performance following 600 h of operational stability at maximum power point in an inert atmosphere at 56 °C (Figure S11, Supporting Information).

To understand the origin of V_{OC} enhancement, we performed time-resolved PL measurements of perovskite films on glass substrates. Consistent with the steady-state PL measurements discussed above, the Cd-$FAPbI_3$ films demonstrated a remarkably long PL lifetime of 1,117 ns, an order of magnitude longer than the control $FAPbI_3$ film (Figure 3c), indicating suppressed non-radiative recombination of charge carriers in the target film. We also performed Ultraviolet photoelectron spectroscopy characterization of the films (Figure S12, Supporting Information). We observed a systematic downshift of perovskite band positions with Cd, minimizing band misalignment with the SnO_2 electron transporter layer (Figure 3d). We hence attribute the enhanced photovoltage to suppressed non-radiative recombination rates in Cd-$FAPbI_3$ and improved band alignment in the device, which together lead to greater electron collection efficiency.[53–56,58]

To gain further insights into charge transfer and trapping in the absorber layer which directly influences the photovoltaic performance,[59–61] we explored Transient Absorption (TA) signals from the films. We monitored a long-lived negative TA signal near the light absorption onset in the µs to ms timescales which is assigned to Ground State Bleaching (Figure S13a, Supporting Information).[62] The experimental kinetic traces were described by the sum of two components: 1) a power law decay attributed to the recombination limited by multiple trapping and release of charge carriers and 2) a second order decay which describes bimolecular recombination of free charge carriers (Figure S13b; Supplementary Note 3, Supporting Information).[63,64] The decays were parametrized by the TA signal amplitude at 1.2 µs and the time the signal decays by half ($t_{50\%}$).

Using Transient Absorption Microscopy (TAM), we explored the spatial heterogeneity in the TA signals between the control and the target samples, using a 785 nm laser diode probe with a spatial resolution of ≈50 µm. We observed higher spatial heterogeneity in both parameters for the target (0.6% Cd) sample compared to the control (Figure S14, Supporting Information). This heterogeneity can be attributed to differences in charge carrier transport and trapping, the main photophysical processes occurring on the monitored *µs* to *ms* timescales.[65] Given comparable uniformity in the deposited films between the two samples,[66]

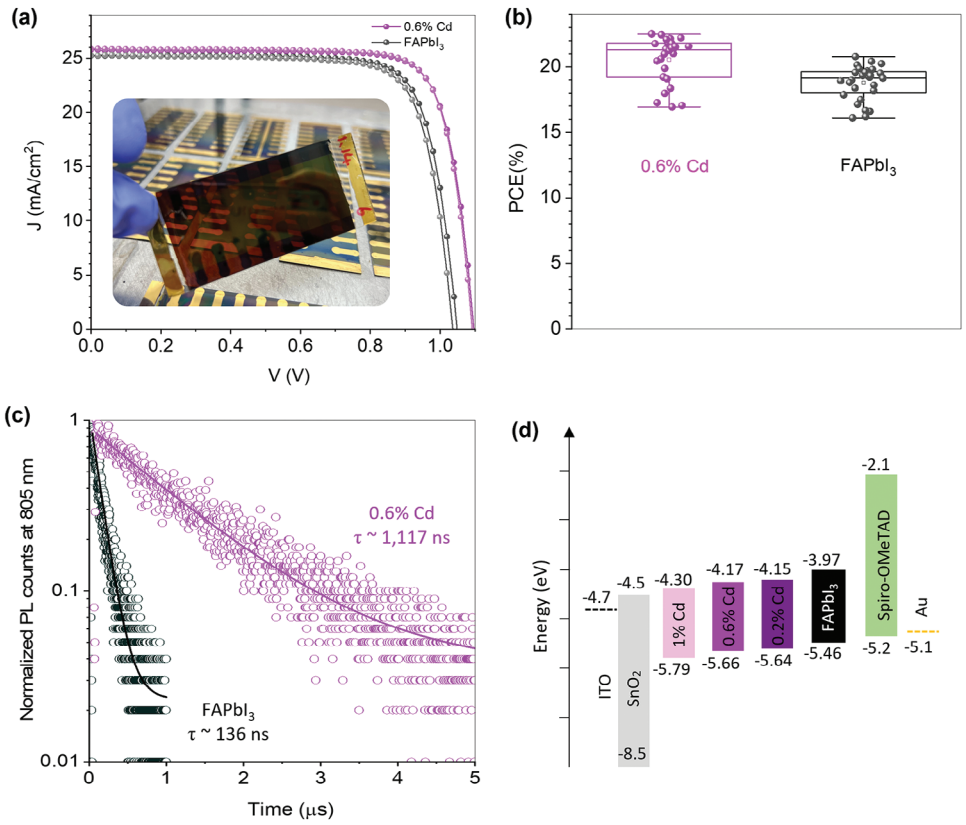

Figure 3. Characterization of perovskite films and solar cells. a,b) *J–V* curves and statistical efficiency data of $FAPbI_3$ PSCs with and without Cd. The inset in panel a) displays an image of perovskite solar cells. c) Transient photoluminescence of $FAPbI_3$ films with and without Cd. d) Energy band diagrams of *n-i-p* $FAPbI_3$ solar cells with and without Cd doped.

these differences between the control and target samples can be linked to changes in compositional and structural features in the perovskite grains or at grain boundaries resulting from Cd doping.[67,68]

Histograms of the extracted parameters from the fits in each pixel are built to quantitatively compare the charge carrier dynamics of the control and target samples. Since our fitting model consists of the sum of two components, we can isolate the power law and the second-order components and extract their parameters separately. Starting with the second-order law component, a histogram of its amplitude (the $\Delta O.D.(t_0)$ associated with the second-order decay) is shown in **Figure** 4a, where we find that between the two samples, the Gaussian distributions almost overlap. The $t_{50\%}$ parameter, interestingly, shows homogenous values within and between the samples – 35 out of 36 pixels in either sample have values of ≈2.6 μs. We conclude that the fraction of excited charges that undergo bimolecular recombination in the μs to ms timescales are not affected by the Cd modification.

Strikingly, the power law component accounts for the change in the overall TA behavior. The histograms of the $\Delta O.D.(t_0)$ and $t_{50\%}$ associated with the power law decay are shown in Figure 4b and c, respectively. In contrast to what we observed in the second-order component, the ΔO.D. at t_0 derived from the power law varies significantly between the samples (Figure 4b,e,f). The histograms show two Gaussian distributions with the means centered at −0.0034 and −0.002 for the control and the target, respectively. We observe heterogeneity in the $t_{50\%}$ parameter of the power law component as well. The distribution of $t_{50\%}$ depicts two distinct Gaussian distributions with two means for the control and the target samples of $10^{-5.14}$ s (7 μs) and $10^{-4.49}$ s (33 μs).

Since power-law decays are characteristic of systems where an energetically exponential tail of trap states is present below near the band edge,[63,64] these observations suggest differences in charge trapping in both samples. Overall, the control $FAPbI_3$ sample showed a higher density of trapped charges (higher amplitude of the ΔO.D. at t_0) and a narrower energetic distribution of trap states (higher α value). Taken together, these results are consistent with an increased availability of trap states near the band edge. The sensitivity of the charge carrier dynamics to trapping makes the difference apparent in the TA signals while it was not observed in the Urbach tail for ground state absorption,[69] suggesting a fairly low trap state density.

In addition, the mean of the $t_{50\%}$ of the power law component is 5-fold shorter for the control sample (7 μs) compared to the Cd-doped target sample (33 μs). As the charge carrier lifetime is shorter in the control sample, we conclude that the trap states near the band edge likely are detrimental recombination centers that lead to reduced charge carrier densities. Our spectroscopic investigation suggests that these states are passivated by the Cd-doping, leading to longer lifetimes of trapped charge carriers, and facilitating the accumulation of high energy charges. This results

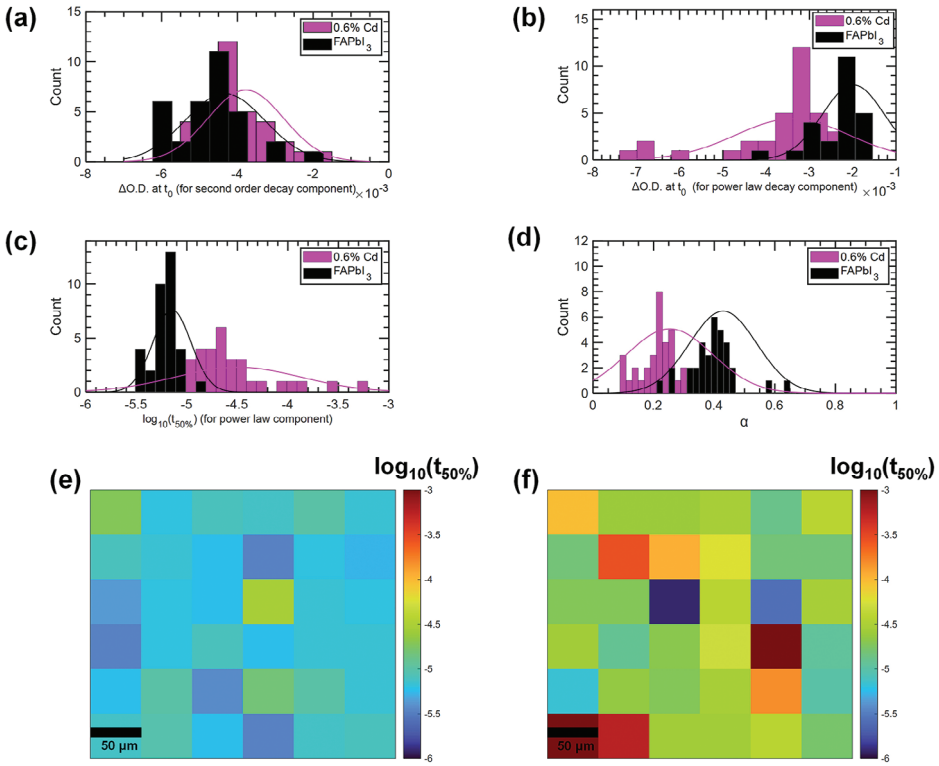

Figure 4. Histograms depicting frequency distributions of the parameters derived from the control ($FAPbI_3$) and target (0.6% Cd) samples: a) ΔO.D. (t_0) derived from second-order component b) ΔO.D. (t_0) derived from power law component c) log10($t_{50\%}$) values derived from the power law component d) Parameter α. e) and f) portray the spatial maps for log10($t_{50\%}$) derived from the power law component for the control and the target, respectively. Scale bars are 50 μm.

in an increased quasi-Fermi level splitting and ultimately an improved V_{oc} in the optimal devices doped with Cd.

3. Conclusion

The development of stable and scalable $FAPbI_3$ perovskite solar cells has been a long-standing challenge due to the polymorphism issue and their sensitivity to fabrication conditions. Here we demonstrated a fully blade-coated $FAPbI_3$ PSCs with a PCE of 22.7% by doping with Cd. Using the compositionally graded film optimization method, we found an optimum doping concentration of Cd, 0.6%, which maximizes radiative recombination rates. Transient absorption microscopy indicated that the target sample exhibits less negative amplitudes (i.e., reduced trapping of charges on the μs – ms timescale) and longer lifetimes (i.e., slower recombination or trap emptying) under illumination. In other words, the trap states in the target sample are more readily filled, leading to increased charge accumulation and higher V_{OC}. These findings open a new avenue for the development of stable and scalable $FAPbI_3$ PSCs, paving the way for the potential commercialization of perovskite solar cells.

Supporting Information

Supporting Information is available from the Wiley Online Library or from the author.

Acknowledgements

The authors thank Solaires Entreprises Inc. and Canada's Natural Sciences and Engineering Research Council (ALLRP 561355-20) for their financial support. D.Y.Z. acknowledges funding from the Chinese Scholarship Council (CSC, grant No. CSC202007030009). M.I.S. is grateful to the NSERC (RGPIN-2020-04239), the Canadian Foundation for Innovation (40326), B.C. Knowledge Development Fund (806169), and the Canada Research Chairs Program (CRC-2019-00297) for financial support. F.T. thanks the Intelligence Introduction Plan of Henan Province in 2021 (CXJD2021008). Y.H. thanks the Japan Society for the Promotion of Science (JSPS) Overseas Research Fellow program for their financial support. R. G. acknowledges the support of the NSERC (RGPIN-2019-05521), the Canada Foundation for Innovation (CFI; 38164), and the B.C. Knowledge Development Fund for operational and infrastructure support.

Conflict of Interest

The authors declare no conflict of interest.

Data Availability Statement

The data that support the findings of this study are available in the supplementary material of this article.

Keywords

ambient air, blade coating, cadmium iodide, formamidinium lead iodide

Received: November 12, 2023
Revised: February 23, 2024
Published online:

[1] G. E. Eperon, S. D. Stranks, C. Menelaou, M. B. Johnston, L. M. Herz, H. J. Snaith, *Energy Environ. Sci.* **2014**, *7*, 982.
[2] J. Jeong, M. Kim, J. Seo, H. Lu, P. Ahlawat, A. Mishra, Y. Yang, M. A. Hope, F. T. Eickemeyer, M. Kim, Y. Jin Yoon, I. Woo Choi, B. Primera Darwich, S. Ju Choi, Y. Jo, J. Hee Lee, B. Walker, S. M. Zakeeruddin, L. Emsley, U. Rothlisberger, A. Hagfeldt, D. Suk Kim, M. Grätzel, J. Young Kim, *Nature* **2021**, *592*, 381.
[3] Best Research-Cell Efficiency Chart | Photovoltaic Research | NREL, https://www.nrel.gov/pv/interactive-cell-efficiency.html (accessed: February 2024).
[4] Q. Han, S. H. Bae, P. Sun, Y. T. Hsieh, Y. Yang, Y. S. Rim, H. Zhao, Q. Chen, W. Shi, G. Li, Y. Yeng, *Adv. Mater.* **2016**, *28*, 2253.
[5] A. Amat, E. Mosconi, E. Ronca, C. Quarti, P. Umari, M. K. Nazeeruddin, M. Grätzel, F. De Angelis, *Nano Lett.* **2014**, *14*, 3608.
[6] W. Shockley, H. J. Queisser, *J. Appl. Phys.* **1961**, *32*, 510.
[7] N. K. Kim, Y. H. Min, S. Noh, E. Cho, G. Jeong, M. Joo, S. W. Ahn, J. S. Lee, S. Kim, K. Ihm, H. Ahn, Y. Kang, H. S. Lee, D. Kim, *Sci. Rep.* **2017**, *7*, 4645.
[8] B. Conings, J. Drijkoningen, N. Gauquelin, A. Babayigit, J. D'Haen, L. D'Olieslaeger, A. Ethirajan, J. Verbeeck, J. Manca, E. Mosconi, F. De Angelis, H. G. Boyen, *Adv. Energy Mater.* **2015**, *5*, 1500477.
[9] J. A. Aguiar, S. Wozny, T. G. Holesinger, T. Aoki, M. K. Patel, M. Yang, J. J. Berry, M. Al-Jassim, W. Zhou, K. Zhu, *Energy Environ. Sci.* **2016**, *9*, 2372.
[10] V. L. Pool, B. Dou, D. G. Van Campen, T. R. Klein-Stockert, F. S. Barnes, S. E. Shaheen, M. I. Ahmad, M. F. A. M. Van Hest, M. F. Toney, *Nat. Commun.* **2017**, *8*, 14075.
[11] T. M. Koh, K. Fu, Y. Fang, S. Chen, T. C. Sum, N. Mathews, S. G. Mhaisalkar, P. P. Boix, T. Baikie, *J. Phys. Chem. C* **2013**, *118*, 16458.
[12] O. J. Weber, D. Ghosh, S. Gaines, P. F. Henry, A. B. Walker, M. Saiful Islam, M. T. Weller, *Chem. Mater.* **2018**, *30*, 3768.
[13] T. Niu, L. Chao, X. Dong, L. Fu, Y. Chen, *J. Phys. Chem. Lett.* **2022**, *13*, 1845.
[14] J. Jeong, M. Kim, J. Seo, H. Lu, P. Ahlawat, A. Mishra, Y. Yang, M. A. Hope, F. T. Eickemeyer, M. Kim, Y. J. Yoon, I. W. Choi, B. P. Darwich, S. J. Choi, Y. Jo, J. H. Lee, B. Walker, S. M. Zakeeruddin, L. Emsley, U. Rothlisberger, A. Hagfeldt, D. S. Kim, M. Grätzel, J. Y. Kim, *Nature* **2021**, *592*, 381.
[15] Z. Xu, L. Zeng, J. Hu, Z. Wang, P. Zhang, C. J. Brabec, K. Forberich, Y. Mai, F. Guo, *Nano Energy* **2022**, *91*, 106658.
[16] A. F. Xu, N. Liu, F. Xie, T. Song, Y. Ma, P. Zhang, Y. Bai, Y. Li, Q. Chen, G. Xu, *Nano Lett.* **2020**, *20*, 3864.
[17] W. Hui, L. Chao, H. Lu, F. Xia, Q. Wei, Z. Su, T. Niu, L. Tao, B. Du, D. Li, Y. Wang, H. Dong, S. Zuo, B. Li, W. Shi, X. Ran, P. Li, H. Zhang, Z. Wu, C. Ran, L. Song, G. Xing, X. Gao, J. Zhang, Y. Xia, Y. Chen, W. Huang, *Science* **2021**, *371*, 1359.
[18] H.-S. Yun, H. W. Kwon, M. J. Paik, S. Hong, J. Kim, E. Noh, J. Park, Y. Lee, S. Il Seok, *Nat. Energy* **2022**, *7*, 828.
[19] T. Zhang, Q. Xu, F. Xu, Y. Fu, Y. Wang, Y. Yan, L. Zhang, Y. Zhao, *Sci. Bull.* **2019**, *64*, 1608.
[20] Z.-A. Nan, L. Chen, Q. Liu, S.-H. Wang, Z.-X. Chen, S.-Y. Kang, J.-B. Ji, Y.-Y. Tan, Y. Hui, J.-W. Yan, Z.-X. Xie, W.-Z. Liang, B.-W. Mao, Z.-Q. Tian, *Chem* **2021**, *7*, 2513.
[21] Y. Huang, X. Lei, T. He, Y. Jiang, M. Yuan, *Adv. Energy Mater.* **2021**, *12*, 2100690.
[22] X. Ling, H. Zhu, W. Xu, C. Liu, L. Pan, D. Ren, J. Yuan, B. W. Larson, C. Grätzel, A. R. Kirmani, O. Ouellette, A. Krishna, J. Sun, C. Zhang, Y. Li, S. M. Zakeeruddin, J. Gao, Y. Liu, J. R. Durrant, J. M. Luther, W. Ma, M. Grätzel, *Angew. Chem., Int. Ed.* **2021**, *60*, 27299.
[23] Y. Zhang, Y. Li, L. Zhang, H. Hu, Z. Tang, B. Xu, N. Park, *Adv. Energy Mater.* **2021**, *11*, 2102538.
[24] S. Masi, A. F. Gualdrón-Reyes, I. Mora-Seró, *ACS Energy Lett.* **2020**, *5*, 1974.
[25] Y. Zhang, S. Seo, S. Yeon Lim, Y. Kim, S.-G. Kim, D.-K. Lee, S.-H. Lee, H. Shin, H. Cheong, N.-G. Park, *ACS Energy Lett.* **2019**, *5*, 360.
[26] Z. Chen, H. Zhang, F. Yao, C. Tao, G. Fang, G. Li, *Cell Rep. Phys. Sci.* **2020**, *1*, 100205.
[27] M. B. Faheem, B. Khan, J. Z. Hashmi, A. Baniya, W. S. Subhani, R. S. Bobba, A. Yildiz, Q. Qiao, *Cell Rep. Phys. Sci.* **2022**, *3*, 100827.
[28] Y. Hou, C. Xie, V. V. Radmilovic, B. Puscher, M. Wu, T. Heumüller, A. Karl, N. Li, X. Tang, W. Meng, S. Chen, A. Osvet, D. Guldi, E. Spiecker, V. R. Radmilovic, C. J. Brabec, Y. Hou, C. Xie, T. Heumüller, A. Karl, N. Li, X. Tang, W. Meng, S. Chen, A. Osvet, C. J. Brabec, V. V. Radmilovic, B. Puscher, D. Guldi, M. Wu, et al., *Adv. Mater.* **2019**, *31*, 1806516.
[29] A. Ray, B. Martín-García, A. Moliterni, N. Casati, K. M. Boopathi, D. Spirito, L. Goldoni, M. Prato, C. Giacobbe, C. Giannini, F. Di Stasio, R. Krahne, L. Manna, A. L. Abdelhady, *Adv. Mater.* **2022**, *34*, 2106160.
[30] J.-Y. Choi, T. L. Alford, C. B. Honsberg, *Langmuir* **2014**, *30*, 5732.
[31] M. Zendehdel, N. Yaghoobi Nia, B. Paci, A. Generosi, A. Di Carlo, *Sol. RRL* **2022**, *6*, 2100637.
[32] Y. Deng, E. Peng, Y. Shao, Z. Xiao, Q. Dong, J. Huang, *Energy Environ. Sci.* **2015**, *8*, 1544.
[33] F. Yang, L. Dong, D. Jang, K. C. Tam, K. Zhang, N. Li, F. Guo, C. Li, C. Arrive, M. Bertrand, C. J. Brabec, H. J. Egelhaaf, *Adv. Energy Mater.* **2020**, *10*, 2001869.
[34] S. Kundu, D. Zhang, A. M. Askar, E. G. Moloney, M. M. Adachi, A. Nadeem, S. Moradi, V. Yeddu, A. L. Abdelhady, O. Voznyy, M. I. Saidaminov, *ACS Mater. Lett.* **2022**, *4*, 707.
[35] M. K. Gangishetty, S. N. Sanders, D. N. Congreve, *ACS Photonics* **2019**, *6*, 1111.
[36] A. Swarnkar, W. J. Mir, A. Nag, *ACS Energy Lett.* **2018**, *3*, 286.
[37] Y. Lin, T. Li, Y. Liu, B. Bahrami, D. Guo, Y. Fang, Y. Shao, A. H. Chowdhury, Q. Wang, Y. Deng, A. Gruverman, T. J. Savenije, Q. Qiao, J. Huang, *Cell Rep Phys. Sci.* **2021**, *2*, 100415.
[38] M. I. Saidaminov, J. Kim, A. Jain, R. Quintero-Bermudez, H. Tan, G. Long, F. Tan, A. Johnston, Y. Zhao, O. Voznyy, E. H. Sargent, *Nature Energy* **2018**, *3*, 648.
[39] S. C. Watthage, Z. Song, N. Shrestha, A. B. Phillips, G. K. Liyanage, P. J. Roland, R. J. Ellingson, M. J. Heben, *ACS Appl. Mater. Interfaces* **2017**, *9*, 2334.
[40] R. Wang, H. Zhang, S. Han, Y. Wu, Z. Hu, G. Zhang, H. Liu, Q. He, X. Zhang, *New J. Chem.* **2021**, *45*, 9243.
[41] Y. Chen, Y. Zhao, Q. Ye, Z. Chu, Z. Yin, X. Zhang, J. You, Y. Chen, Y. Zhao, F. Ye, Z. M. Chu, Z. G. Yin, X. W. Zhang, *J. Semicond.* **2019**, *40*, 122201.
[42] H. Zhong, X. Liu, M. Liu, S. Yin, Z. Jia, G. Fu, S. Yang, W. Kong, *Nano Energy* **2023**, *105*, 108014.
[43] T. Xu, W. Xiang, D. J. Kubicki, Y. Liu, W. Tress, S. Liu, T. Xu, W. Xiang, Y. Liu, S. Liu, *Adv. Sci.* **2022**, *9*, 2204486.
[44] S. Moradi, S. Kundu, M. Rezazadeh, V. Yeddu, O. Voznyy, M. I. Saidaminov, *Commun. Mater.* **2022**, *3*, 13.
[45] N. K. Tailor, M. Abdi-Jalebi, V. Gupta, H. Hu, M. I. Dar, G. Li, S. Satapathi, *J. Mater. Chem. A* **2020**, *8*, 21356.
[46] P. Raval, R. M. Kennard, E. S. Vasileiadou, C. J. Dahlman, I. Spanopoulos, M. L. Chabinyc, M. Kanatzidis, G. N. Manjunatha Reddy, *ACS Energy Lett.* **2022**, *7*, 1534.
[47] Q. Wang, B. Chen, Y. Liu, Y. Deng, Y. Bai, Q. Dong, J. Huang, *Energy Environ. Sci.* **2017**, *10*, 516.
[48] S. K. Yadavalli, Y. Zhou, N. P. Padture, *ACS Energy Lett.* **2017**, *3*, 63.

[49] W. Li, S. K. Yadavalli, D. Lizarazo-Ferro, M. Chen, Y. Zhou, N. P. Padture, R. Zia, *ACS Energy Lett.* **2018**, *3*, 2669.
[50] M. I. Saidaminov, A. L. Abdelhady, G. Maculan, O. M. Bakr, *Chem. Commun.* **2015**, *51*, 17658.
[51] X. Wang, Z. Han, F. Gao, C. Luo, Q. Zhao, *Sol. RRL* **2022**, *6*, 2100973.
[52] Y. Liu, C. Tao, Y. Cao, L. Chen, S. Wang, P. Li, C. Wang, C. Liu, F. Ye, S. Hu, M. Xiao, Z. Gao, P. Gui, F. Yao, K. Dong, J. Li, X. Hu, H. Cong, S. Jia, T. Wang, J. Wang, G. Li, W. Huang, W. Ke, J. Wang, G. Fang, *Nat. Commun.* **2022**, *13*, 7425.
[53] H. Wei Qiao, S. Yang, Y. Wang, X. Chen, T. Yu Wen, L. Juan Tang, Q. Cheng, Y. Hou, H. Zhao, H. Gui Yang, H. W. Qiao, X. Chen, T. Y. Wen, L. J. Tang, Q. Cheng, Y. Hou, H. G. Yang, S. Yang, Y. Wang, H. Zhao, *Adv. Mater.* **2019**, *31*, 1804217.
[54] Y. Wu, X. Yang, W. Chen, Y. Yue, M. Cai, F. Xie, E. Bi, A. Islam, L. Han, *Nat. Energy* **2016**, *1*, 16148.
[55] Y. Hou, X. Chen, S. Yang, C. Li, H. Zhao, H. Gui Yang, Y. Hou, X. Chen, S. Yang, C. Li, H. G. Yang, H. Zhao, *Adv. Funct. Mater.* **2017**, *27*, 1700878.
[56] Y. Hou, X. Chen, S. Yang, Y. L. Zhong, C. Li, H. Zhao, H. G. Yang, *Nano Energy* **2017**, *36*, 102.
[57] Y. Niu, Y. Peng, X. Zhang, Y. Ren, R. Ghadari, J. Zhu, G. Tulloch, H. Zhang, P. Falaras, L. Hu, *ACS Energy Lett.* **2022**, *7*, 3104.
[58] Z. Yang, Z. Yu, H. Wei, X. Xiao, Z. Ni, B. Chen, Y. Deng, S. N. Habisreutinger, X. Chen, K. Wang, J. Zhao, P. N. Rudd, J. J. Berry, M. C. Beard, J. Huang, *Nat. Commun.* **2019**, *10*, 4498.
[59] J. Jean, P. R. Brown, R. L. Jaffe, T. Buonassisi, V. Bulović, *Energy Environ. Sci.* **2015**, *8*, 1200.
[60] D. P. Ostrowski, M. S. Glaz, B. W. Goodfellow, V. A. Akhavan, M. G. Panthani, B. A. Korgel, D. A. Vanden Bout, *Small* **2010**, *6*, 2832.
[61] J. P. Correa-Baena, Y. Luo, T. M. Brenner, J. Snaider, S. Sun, X. Li, M. A. Jensen, N. T. P. Hartono, L. Nienhaus, S. Wieghold, J. R. Poindexter, S. Wang, Y. S. Meng, T. Wang, B. Lai, M. V. Holt, Z. Cai, M. G. Bawendi, L. Huang, T. Buonassisi, D. P. Fenning, *Science* **2019**, *363*, 627.
[62] J. Yang, X. Wen, H. Xia, R. Sheng, Q. Ma, J. Kim, P. Tapping, T. Harada, T. W. Kee, F. Huang, Y. B. Cheng, M. Green, A. Ho-Baillie, S. Huang, S. Shrestha, R. Patterson, G. Conibeer, *Nat. Commun.* **2017**, *8*, 14120.
[63] R. Godin, X. Ma, S. González-Carrero, T. Du, X. Li, C. T. Lin, M. A. McLachlan, R. E. Galian, J. Pérez-Prieto, J. R. Durrant, *Adv. Opt. Mater.* **2018**, *6*, 1701203.
[64] A. D. Wright, R. L. Milot, G. E. Eperon, H. J. Snaith, M. B. Johnston, L. M. Herz, A. D. Wright, R. L. Milot, G. E. Eperon, H. J. Snaith, M. B. Johnston, L. M. Herz, *Adv. Funct. Mater.* **2017**, *27*, 1700860.
[65] J. Shi, Y. Li, Y. Li, D. Li, Y. Luo, H. Wu, Q. Meng, *Joule* **2018**, *2*, 879.
[66] E. G. Moloney, D. Thrithamarassery Gangadharan, V. Yeddu, D. Zhang, S. Moradi, A. M. Askar, M. M. Adachi, D. C. Leitch, M. I. Saidaminov, *Chem. Mater.* **2022**, *34*, 4394.
[67] J. M. Snaider, Z. Guo, T. Wang, M. Yang, L. Yuan, K. Zhu, L. Huang, *ACS Energy Lett.* **2018**, *3*, 1402.
[68] S. Deng, D. D. Blach, L. Jin, L. Huang, *Advanced Energy Materials* **2020**, *10*, 1903781.
[69] E. Serpetzoglou, I. Konidakis, G. Kakavelakis, T. Maksudov, E. Kymakis, E. Stratakis, *ACS Appl. Mater. Interfaces* **2017**, *9*, 43910.